SUBCOOLED FLOW BOILING HEAT TRANSFER ENHANCEMENT IN MICROCHANNELS/TUBES WITH MODIFICATIONS OF SURFACE CHARACTERISTICS WITH MICRO/NANO STRUCTURES AND FILMS

by

MASOUMEH NEDAEI

Submitted to the Graduate School of Engineering and Natural Sciences
in partial fulfillment of
the requirements for the degree of
Master of Science

Sabanci University

December 2015

SUBCOOLED FWW IDILING HEAT TRANSFER ENHANCEMENT IN MICROCHANNELS!IUBES WITH MODIFICATIONS OF SURFACE CHARACTERISTICS WITH MICRO/NANO STRUCTURES AND FILMS

APPROVED BY:

Asst. Prof. Dr. / Assoe. Pt'Of Dr. / Pro£ Dr. Ali Ko ar

(Thesis Supervisor)

Asst. Prof Dr. / Assoc. Pw£ Dr. / Pw£ Dr. Gozde Ozaydin ince

Asst. Pw£ Dr. / Assoc. Prof Dr. / Pwf Dr. Tansel Karabacak

DATE OF APPROVAL: 3011212015

ABSTRACT

SUBCOOLED FLOW BOILING HEAT TRANSFER ENHANCEMENT IN MICROCHANNELS/TUBES WITH MODIFICATIONS OF SURFACE CHARACTERISTICS WITH MICRO/NANO STRUCTURES AND FILMS

MASOUMEH NEDAEI

MSc. Thesis, December 2015

Supervisor: Prof. Dr. Ali Koşar

Keywords: Heat transfer enhancement, Subcooled flow boiling, Enhanced surfaces, Microchannels/tubes

In this study, subcooled flow boiling was experimentally investigated in micro tubes/channels, whose surfaces were enhanced by various methods. In all the experiments, deionized (DI) water was used as the working fluid. In the first study, initiated chemical vapor deposition (iCVD) method was employed to coat the inner walls of stainless steel hypodermic microtubes having inner diameter of 502 μm with polyhydroxyethylmethacrylate (pHEMA)/polyperfluorodecylacrylate (pPFDA) coatings. This coating altered wettability along the surface of the microchannels and also offered high porosity. To investigate the effect of wettability, the experiments were accomplished for both hydrophilic and hydrophobic ends of the microtubes such that one end corresponded to the most hydrophilic (pHEMA) location, while the other end

corresponded to the most hydrophobic (pPFDA) location. The results were compared to the results with the bare surface microtube. The experimental results revealed a remarkable increase in subcooled boiling heat transfer with the coatings, while the highest heat transfer coefficients were attained for the pHEMA coated (hydrophobic inlet and hydrophilic outlet) outlet case with a maximum heat transfer enhancement ratio of ~64%. The reason for the enhanced heat transfer with the coated microtubes can be attributed to the increased nucleation site density and bubble release as well as enhanced convection and bubble motion near the surface due to the variation in wettability along the length. The results showed that gradient pHEMA/pPFDA coatings obtained by iCVD method can be utilized as a viable surface enhancement method in microscale cooling applications.

In the second study, a horizontal microchannel made of Aluminum (Al) with a length of 14 cm, width of 1.5 cm, and depth of 500 μm was utilized to investigate subcooled boiling heat transfer. Environmentally friendly and simple methods of sanding with sandpapers in different grit sizes and immersion in boiling DI water were used to prepare the micro and nano structured (hierarchical) Al alloy 2024 plates (150 × 150 mm) which were integrated near the exit of the microchannel. The experiments were carried out at different mass fluxes of 70, 100, and 125 kg/m^2s. The results revealed that plates sanded with grit sizes of 400 and 1000 enhanced heat transfer coefficients while plates sanded with grit sizes of 36 and 60 deteriorated heat transfer coefficients compared to the untreated plate. The reason for heat transfer enhancement was related to an increase in both the heating surface area and active nucleation sites. A high speed camera was used for visualizing bubble departures in boiling experiments.

ÖZET

MİKRO/NANO YAPILAR VE FİLMLERLE YÜZEY KARAKTERİSTİĞİ DEĞİŞTİRİLMİŞ MİKROKANAL/ TÜPLERDE DOYMAMIŞ AKIŞ KAYNAMA ISI TRANSFERİ ARTIRILMASI

MASOUMEH NEDAEI

YÜKSEK LİSANS TEZİ, Aralık 2015

Danışman: Prof. Dr. Ali Koşar

Anahtar kelimeler: Isı transferi artırılması, Doymamış akış kaynaması, Geliştirilmiş yüzeyler, Mikrokanallar/tüpler

Bu çalışmada, doymamış akış kaynaması, yüzeyleri çeşitli metodlarla geliştirilmiş mikrotüpler/kanallarda deneysel olarak araştırılmıştır. Tüm deneylerde, çalışma sıvısı olarak deiyonize (DI) su kullanılmıştır. İlk çalışmada, 502 μm iç çaplı hipodermik paslanmaz çelik mikrotüplerin iç duvarlarını polihidroksietilmetakrilat (pHEMA)/poliperflorodesilakrilat (pPFDA) kaplamak için başlatılmış kimyasal buhar biriktirme metodu kullanılmıştır. Bu kaplama, mikrokanalların yüzeyi boyunca ıslanabilirliği değiştirmiş ve aynı zamanda yüksek gözeneklilik sunmuştur.

Islanabilirliğin etkisini araştırmak için deneyler, mikrotüplerin hem hidrofobik hem hidrofilik uçlarında yapılmıştır ki bu uçların biri en hidrofilik yere (pHEMA) ve diğeri en hidrofobik yere (pPFDA) karşılık gelmektedir. Sonuçlar, yüzeyi kaplamasız mikrotüp sonuçlarıyla karşılaştırılmıştır. Deneysel sonuçlar kaplamalarla doymamış akış kaynama ısı transferinde kayda değer bir artış olduğunu ortaya çıkarmıştır ancak en yüksek ısı transferi katsayılarına pHEMA kaplanmış çıkış kısmında (hidrofobik giriş ve hidrofilik çıkış) maksimum % 64 artış oranıyla ulaşılmıştır. Kaplanmış mikrotüplerde ısı transferi artışının sebebi çekirdeklenme bölgesi yoğunluğu, baloncuk salınması, artırılmış konveksiyon, ve baloncuk hareketidir ve bunun da sebebi uzunluk boyunca ıslanabilirliğin değiştirildiğidir. Sonuçlar göstermiştirki iCVD metoduyla elde edilmiş olan gradyan şeklinde pHEMA/pPFDA kaplaması mikro boyutta soğutma uygulamaları için kullanılabilir bir yüzey geliştirme metodu olarak değerlendirilebilir.

İkinci çalışmada, 14 cm uzunlukta, 1.5 cm genişlikte, ve 500 μm derinlikte olan bir aluminyum 2024 alaşımından yapılmış bir yatay mikrokanal, doymamış kaynama ısı transferi araştırılması için kullanılmıştır. 150 × 150 mm boyutlarında mikro ve nano yapılı olan aluminyum plakaları hazırlamak için, farklı kum tanesi boyutunda zımparalayarak ve kaynayan DI suya batırarak çevreye zarar vermeyen ve basit yöntemler kullanılmıştır. Deneyler 70, 100, ve 125 kg/m^2s olan farklı kütle akılarında gerçekleştirilmiştir. Sonuçlar 400 ve 1000 kum tanesi boyutlarla zımparalanmış plakalarda ısı transferi katsayılarında artış gösterirken, 36 ve 60 kum tanesi boyutlarla zımparalanmış plakalar, işlem görmemiş plakalara göre ısı transferi kat sayılarında bozulma göstermiştir. Isı transferi artışı, artırılmış ısıtma yüzey alanı ve daha aktif çekirdeklenme alanı sebebiyledir. Görüntüleme çalışması mikro ve nano yapılı plakalarda baloncukların ayrılmasını ve ortaya çıkan baloncukların boyutunu göstermek amacıyla yapılmıştır.

ACKNOWLEDGEMENT

First, I would like to express my gratitude to Prof. Dr. Asif Şabanoviç to give me the opportunity to learn many things from his constructive comments and recommendations.

Secondly, I would like to acknowledge my advisor, Prof. Dr. Ali Koşar, for his continuous support and guidance through my studies with him. I would not have been able to do this work without him. I would also like to mention my appreciation to my thesis dissertation defense jury members, Assis. Prof. Gozde Ozaydin Ince and Assoc. Prof. Tansel Karabacak, who honored me by accepting to be my defense jury members.

Special thanks go to my colleagues in Microthermal and Microfluidics Systems laboratory due to their help and guidance, especially to Mostafa Shojaeian and Mehrdad Karimzadehkhouei. I would also like to thank Dr. Meltem Sezen and Ali Tufani for their great assistance with characterization of the samples used in my studies.

Last but not least, I wish to thank my lovely family for their encouragement and assurance all the time.

TABLE OF CONTENTS

LIST OF FIGURES

LIST OF TABLES

LIST OF SYMBOLS AND ABBREVIATIONS

A_c = cross-sectional area (m^2)

c_p = specific heat of liquid (kJ/kg K)

d = channel diameter (m)

f = friction factor (-)

G= mass flux (kg/m^2s)

h = heat transfer coefficient (W/m^2 K)

h_{FG}= latent heat of vaporization (J/kg K)

k = thermal conductivity (W/m K)

L = length (m)

$\dot{m}$ = mass flow rate (kg/s)

Nu = Nusselt number (-)

Pr = Prandtl number (-)

P = electrical power (W)

q" = heat flux (W/m^2)

$\dot{q}$ = volumetric heat generation (W/m^3)

$\dot{Q}_{loss}$ = heat loss (W)

$\dot{Q}$ = volumetric flow rate (m^3/s)

r = radius of the microtube (m)

R = resistance (Ω)

Re = Reynolds number (-)

T = temperature (°C)

u = flow velocity (m/s)

x = thermocouple location (m)

x_e = local exit vapor quality (-)

Greek symbols

μ = dynamic viscosity (kg/ms)

ρ = density (kg/m^3)

Subscripts

amb = ambient

f = fluid

h = hydraulic, heated

i = inlet, inner

o = outer

s = surface

sat = saturation

tg = grease

th = thermocouple

tot = total

tp = two phase

w = wall

CHAPTER 1

LITERATURE REVIEW

1.1 Flow Boiling

Boiling occurs on surfaces heated above the saturation temperature. The saturation temperature of any liquid can be defined as the temperature at which the vapor pressure reaches the ambient pressure. Boiling is classified into two types based on the bulk motion: pool boiling and flow boiling. When there is no bulk fluid motion, pool boiling conditions exist. In pool boiling, relative motion of the fluid can be attributed to natural convection currents or the displacement of the vapor bubbles from the surface. In flow boiling, the liquid is forced to move along the heated surface. Therefore, the liquid has a relative velocity with respect to the heated surface. In this case, boiling happens when the wall temperature of the channel is higher than the saturation temperature [1]. In this thesis, flow boiling will be studied.

Flow boiling itself is classified into two categories: subcooled boiling and saturated boiling. Saturated flow boiling occurs when the bulk liquid temperature is the saturation temperature, and the emerging bubbles detach from the heated surface and grow according to the applied heat to the heated surfaces. The temperature difference between the wall and saturation temperature is called wall superheat and defined as $\Delta T_{sat} = T_w - T_{sat}$. Saturated flow boiling is also classified into nucleate boiling, convective boiling, and their combination. In nucleate boiling, heat transfer takes place via bubbles generated at active nucleation sites on the heated surfaces, while a thin liquid film formed between the heated surface and the vapor in convective boiling. Subcooled flow boiling happens when the bulk liquid temperature is below the saturation temperature of the liquid, while the heated surface temperature is higher than the saturation temperature. Subcooling is defined as the temperature difference between wall temperature and fluid temperature as $\Delta T_{sub} = T_{sat} - T_f$ [2].

1.2 Heat transfer enhancement techniques in mini/micro scale

Flow boiling in mini/micro scale has been widely employed in many applications where high-flux heat dissipation is inevitable. Such applications include microreactors [3], aerospace applications [4] , high performance computers [5], microelectronics [6], bioengineering [7], chemical engineering [8], fuel cells [9], and drug delivery [10]. Researchers have been therefore suggested many methods to improve flow boiling heat transfer in micro channels via altering heating surface characteristics like roughness, wettability or micro/nano structures.

Berenson et al. [11] investigated the effects of roughness on n-pentane flow boiling experiments. They found no significant effects on maximum nucleate-boiling heat flux and the film-boiling curve while nucleate heat transfer coefficient of the roughened surface increased up to 5 times compared to the bare surface. Benjamin and Balakrishnan [12] performed pool boiling experiments using different liquids including distilled water, acetone, n-hexane, and carbon tetrachloride. They utilized surfaces with various roughnesses with roughness parameters of 0.2, 0.52, 0.89, and 1.17 μm. They polished stainless steel and aluminum surfaces with various grades of emery paper to obtain roughened surfaces. The results showed that nucleation site density was dependent on the surface roughness. Kang [13] performed saturated pool boiling experiments to test the effects of the surface roughness on heat transfer enhancement. They used water as the working liquid. The results demonstrated higher HTC with increased surface roughness at a given superheat compared to the plain surface due to more cavities produced on the rough surface. However, there was no significant increase in pool boiling heat transfer with more roughened surfaces in the horizontal tubes. The reason was attributed to more bubble slugs produced on the surfaces as heat flux was increased and weak liquid agitation made in horizontal tubes. In contrast, when changing the orientation of the tube to vertical, the effects of HTC were more pronounced with more roughened surfaces due to more liquid agitation and smaller bubble slugs. Jung and Kwak [14] carried out subcooled boiling experiments on sub-micron roughened silicon surfaces using FC-72 as the working fluid. They used anodization with HF (hydrofluoric acid) based electrolyte and DMF (dimethylforamide) base for preparing the samples. They observed an enhancement in nucleate boiling heat transfer with roughened surfaces which was due to more nucleation sites. Alam et al. [15] investigated the effects of surface roughness on flow boiling heat transfer using

heat sinks with different microgap dimensions including 500, 300, and 200 μm. They performed their experiments using deionized water at two mass flux values of 390 and 650 kg/m^{2}s. They reported that heat transfer rates and bubble nucleation site density increased with surface roughness. Wu et al. [16] studied the effects of hydrophilic titanium oxide (TiO_2) coated surfaces on saturated pool boiling of water and FC-72. They obtained an enhancement of 91.2% with FC-72. They also utilized silicon oxide (SiO2) coated surfaces of similar surface topology to investigate the effects of roughness. The experimental results proved that wettability of TiO_2 coated surfaces is an advantage for heat transfer enhancement. McHale and Garimella [17] investigated pool boiling experiments of FC-77 on smooth and roughened surfaces made of aluminum. They prepared smooth surfaces by mechanical polishing and roughened surfaces by electrical discharge machining. They obtained peak to peak roughness values of 0.03 and 5.89 μm for polished and roughened surfaces, respectively. The experimental results illustrated that more heat transfer enhancement could be achieved using rough surfaces. Ammerman and You [18] investigated convective boiling heat transfer using a single-channel heater and FC-87 as the working fluid at the mass fluxes from 500 to 5000 kg/m^{2}s. They performed their experiments on the heated section of the length of 8 cm with and without microporous surface coating. The coating results revealed significant enhancement in heat transfer. Lee et al. [19] exploited anodizing method for coating aluminum alloy (6061) surfaces to provide nano porous structures. They carried out nucleate pool boiling experiments using water as the working fluid. The results revealed that nucleate pool boiling heat transfer increased with nano porous surfaces at heat fluxes smaller than 60 kW/ m^2. Gulliksen et al. [20] studied boiling heat transfer performance of porous coatings for possible applications in electronics cooling. They observed a reduction in superheat incipience as well as an increase in the heat transfer coefficient compared to the polished Silicon surfaces. Sarwar et al. [21] tested different aluminum porous coatings inside a tube at mass fluxes between 100 and 300 kg/m^{2}s and subcooling of 50°C and 75°C. The results showed that Al_2O_3 coatings offered higher heat transfer coefficients (HTC) than TiO_2 coatings. In the studies conducted by Sun et al. [22,23] it was shown that small (hydraulic diameter of 2.27mm) and minichannels (hydraulic diameters of 0.49, 0.93 and 1.26 mm) enhanced by microporous coatings resulted in higher two phase heat transfer in flow boiling of water and FC 72. The results showed 3 times and 7-10 times heat transfer enhancement with coated small and minichannels, respectively, compared to plain surface channels.

Phan et al. [24] studied the effects of surface wettability in subcooled pool boiling of water. They coated stainless steel ribbon surfaces by nanoparticles including SiOx, SiOC, TiO_2, Pt, Fe_2O_3, and Teflon in order to change the static contact angles from 22º ta 112º. The techniques used to prepare these samples were 'Metal-Organic Chemical Vapor Deposition' (MOCVD), 'Plasma Enhanced Chemical Vapor Deposition' (PECVD), and 'Nanofluids Nucleate Boiling Deposition' (NNBD). The best heat transfer performance belonged to the surfaces with static contact angle of 0º or 90º. Hendricks et al. [25] produced nanostructured surfaces by depositing ZnO nanostructures on Cu and Al surfaces. The experiments with nanostructured surfaces revealed higher augmentation in pool boiling heat transfer compared to a bare Al and Si surfaces. Forrest et al. [26] applied silica nanoparticle thin film coatings on nickel wires using layer-by-layer deposition method. The treatments on nickel wires changed wettability of the coated surfaces as shown from surface characterization results. The pool boiling experiments demonstrated an improvement in heat transfer coefficient with decreasing wettability. Thin film coatings modified with fluorosilane offered higher HTC with an increase over 100%. Stutz et al. [27] used ionic nanoparticles (γ-Fe_2O_3) deposition on a 100 μm diameter platinum wire to produce a nanoporous layer. They exploited vigorous boiling and electrophoresis for coating the samples. The pool boiling experiments for both water and pentane demonstrated degradation in heat transfer coefficient relative to a plain surface wire. The reason was attributed to increased thermal resistance, which was affected by increasing the layer thickness. Morshed et al. [28] utilized Cu-Al_2O_3 nanocomposite coatings over a microchannel of 672 μm hydraulic diameter to study water flow boiling at different mass fluxes. Electrodeposition technique was used to coat the microchannels. They reported two phase heat transfer enhancement from ~30% to ~120% with coated microchannels. Khanikar et al. [29] employed rectangular microchannels coated with carbon nanotubes (CNTs). They observed an extension in boiling curve with CNTs coated microchannels. However, the morphology of CNTs coated surfaces were changed after repetitions of tests at high flow velocities leading to a decline in CHF. Şeşen et al. [30] accomplished pool boiling experiments by integrating an array of copper nanorods having an average diameter of ~100 nm and length of ~500 nm on a silicon wafer surface coated with a planar copper thin film. The results of the nanostructured surfaces displayed an enhancement of 100% in boiling heat transfer. Chen et al. [31] and Morshed et al. [32] showed that nanowire coatings could be an effective method for enhancing heat transfer

rate. Chen et al. [31] reached a pool boiling heat transfer enhancement of over 100% using both Si and Cu nanowires regardless of different thermal conductivities. They concluded that boiling heat transfer is affected by bubble dynamics rather than heat conduction. Morshed et al. [32] provided copper nanowire (CuNWs) coatings on the bottom surface of the microchannels having a hydraulic diameter of 672 μm. Electrochemical deposition method was utilized to enhance the surfaces of microchannels. They performed flow boiling experiments at different mass fluxes and subcoolings and provided an enhancement up to ~56% using these coatings. Saeidi and Alemrajabi [33] perused the effects of differently coated aluminum surface on pool boiling heat transfer. They prepared the coatings by sandblasting, etching and anodizing in electrolytes containing chromic and sulfuric acid in different durations. The highest heat transfer coefficients were obtained from weakly etched surfaces (with an increase of 159% relative to the uncoated surface). Kaya et al. [34] coated inner walls of mini/microtubes with polyhydroxyethylmethacrylate (pHEMA) of ~30 nm thickness. Water flow boiling experiments were carried out using microtubes having inner diameters of 249, 507 and 998 μm at mass fluxes of 10000 and 13000 kg/m^{2}s. The pHEMA coated microtubes featured a maximum enhancement of 109% in HTC, proving that pHEMA coated mini/microtubes could be a successful method for flow boiling heat transfer enhancement. Taha et al. [35] investigated effects of the coating thickness on pHEMA coated microtubes. They considered different coating thicknesses of 50, 100 and 150 nm on mini/microtubes of the same dimension as in the study of Kaya et al. [34]. They performed water flow boiling experiments at mass fluxes of 5000 and 20000 kg/m^{2}s. The results showed that thicker coatings lead to more heat transfer enhancement.

Frost and Kippenhan [36] utilized water with and without different concentrations of surfactant “Ultra Wet 60L” to investigate boiling heat transfer in a vertical annulus. They observed an increase in heat transfer rate, which was associated with reduction in the surface tension. Wen and Wang [37] used different surfactant containing 95% sodium dodecyl sulfate (SDS), Triton X-100 and octadecylamine to study pool boiling of water and acetone. They considered various concentrations of surfactant solution on both smooth and roughened surfaces. They obtained an augmentation in boiling heat transfer for both smooth and rough surfaces while using SDS solution and Triton X-100, respectively. For studying the effects of wettability in the absence of microscale roughness, Jo et al. [38] tested three different wettability surfaces including

heterogeneous (hydrophobic dots on a hydrophilic surface) and hydrophilic and hydrophobic surfaces to study nucleate boiling heat transfer. The experiments revealed that hydrophobic surfaces had higher HTC in the low heat flux regime compared to hydrophilic surfaces. However, heterogeneous surfaces had the best heat transfer enhancement compared to homogeneous surfaces. Betz et al. [39] accomplished 6 different surfaces containing hydrophilic, hydrophobic, superhydrophilic, superhydrophobic, biphilic and superbiphilic to study pool boiling of water. They juxtaposed (super) hydrophilic and (super) hydrophobic regions to provide (super) biphilic surfaces. Biphilic surfaces augmented heat transfer compared to uniform wettability surfaces while superbiphilic surfaces had the highest HTC exceeding 150 kW/m^2K.

From the abovementioned studies, it can be realized that micro/nano structured surfaces as well as nanofilm deposition on different surfaces have been considered as an effective method to augment boiling heat transfer. Motivated from such studies, in this thesis, polyhydroxyethylmethacrylate (pHEMA) and polyperfluorodecylacrylate (pPFDA) coatings were used in Chapter 2 to enhance inner walls of the microtubes with inner diameters of 502 µm. The initiated chemical vapor deposition (iCVD) method was used to coat the inner walls of the microtubes. Flow boiling experiments were carried out at high mass flux of 9500 kg/m^2s using water as the working fluid. Experimental results were obtained using the most hydrophobic and the most hydrophilic locations of the microtubes as the test sections to investigate the effects of wettability.

In Chapter 3, micro and nano structured aluminum (Al) plates were utilized to study subcooled flow boiling experiments in a rectangular microchannel. The micro and nano structured (hierarchical) plates were implemented near the exit of the microchannel having dimensions of 14 cm (length)x 1.5 cm (width) x 500 µm (depth). Two simple techniques used to prepare the plates are: 1) Randomly sanding of Al alloy plates with different grit sizes ranged from 36 to 1000 to form microroughened plates. 2) Immersion in boiling DI water for 1 minute to have nanoroughnesses. Experiments were carried out at different mass fluxes of 70, 100, and 125 kg/m^2s using DI water. The results showed that plates sanded with grit sizes of 400 and 1000 enhanced heat transfer. On the other hand, plates roughened with grit sizes of 36 and 60 deteriorated heat transfer compared to the untreated plate. The reason for heat transfer augmentation with plates sanded with grit sizes of 400 and 1000 can be linked to increased surface area and

more active nucleation site densities. Visualization was performed by a high speed camera to support the experimental results and visualize nucleation from surfaces.

CHAPTER 2

Enhancement of Flow Boiling Heat Transfer in pHEMA/pPFDA Coated Microtubes with Longitudinal Variations in Wettability

2.1 Sample Preparation

Polymer thin film deposition onto complex geometries, such as micro/nano channels or porous structures, is a very problematic task. Conventional solution based polymerization techniques are not able to coat polymer on all edges of these structures due to the liquid surface tension and wetting effect. However, vapor deposition techniques enable the deposition of polymer thin films with reasonable conformality and high purity which are necessary for polymeric microchannel applications. Uniform coating of metallic microtubes with an inner diameter of 502 μm is a very challenging task via solution based polymerization methods. Besides, solution techniques can leave many residuals behind, which decrease the uniformity of the coating and performance of microchannel. Thus, initiated chemical vapor deposition (iCVD) technique is proposed to deposit gradient poly (hydroxyethyl methacrylate) p (HEMA)/ poly (perfluorodecylacrylate) p (PFDA) into metal microtubes in order to enhance conformality and homogeneity. Due to being solventless and one step process of iCVD, it is possible to coat very complex geometries. Furthermore, iCVD technique compared to other techniques provides depositing polymer on delicate substrates that results in polymeric thin films with good purity [40].

iCVD is a type of hot wire chemical vapor deposition technique (HWCVD) whose crucial advantages were proven in many studies [40–42]. Free radical polymerization, which is composed of three steps, initiation, propagation and termination, takes place in the iCVD technique as shown in Fig. 1 [40]. The monomer, which is heated to a certain temperature in order to obtain enough vapor pressure, and initiator molecules are delivered into the chamber simultaneously. Firstly, the initiator is decomposed into radical molecules by heated filaments. The heated monomers are directly adsorbed by the cool stage without any decomposition. The radical molecules then attack the C=C bonds of the monomers, initiating the polymerization, and continuous delivery of the monomer molecules to the surface enables propagation reactions. There are many

kinetic studies on experimental parameters of iCVD, which can be tuned to obtain enhancement in the film composition, conformality, and growth rate, such as chamber pressure, monomer/initiator flowrate, substrate temperature, and filament temperature [43]. Gradient deposition was achieved by delivering the HEMA and PFDA monomers to the chamber from the opposite directions so that the HEMA/PFDA ratio of the polymer gradually increased from one end to the other. The flowrate of HEMA and PFDA monomers were respectively set to 0.9 and 0.3 sccm, while the ethylene glycoldimethacrylate (EGDMA) (as a crosslinker) flowrate was 0.08 sccm. During iCVD, the substrate and filament temperatures were kept at 25 °C and 250 °C. The chamber pressure was maintained at 300 mTorr. All depositions for microtubes with diameters of 502 µm were carried out for 30 minutes in order to obtain 150 nm thick films on bare Si wafer.

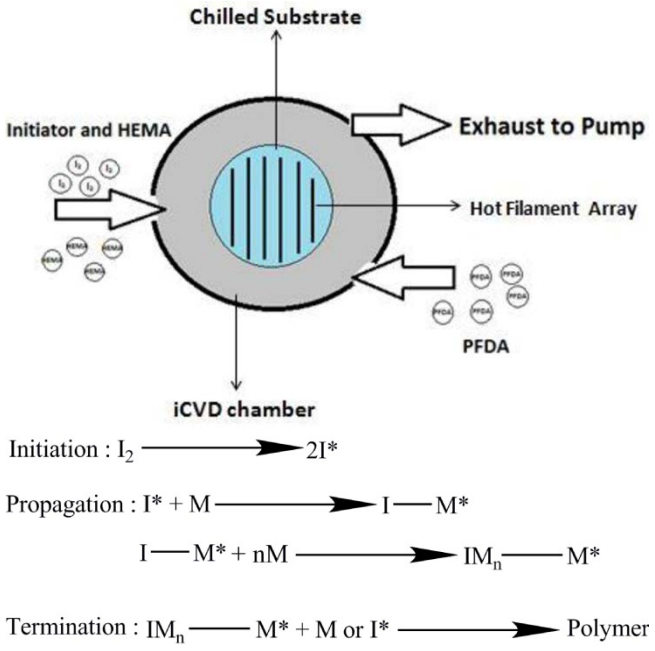

Fig.1. A radical molecule formation, polymer growth, and polymerization in iCVD method including three main steps, initiation, propagation and termination

2.2 Complementary Analysis

2.2.1 Raman Spectroscopy

Raman spectroscopy is commonly used to obtain fingerprint of the identified molecules in a sample. A laser light used in Raman scattering interacts with excitations in the sample and provides up or down shifts in the energy of laser photons. Raman spectroscopy method was utilized to analyze gradient pHEMA/pPFDA coatings. Raman spectral analysis was performed at the Renishaw in Via Raman microscope with laser and grating specifications of a 532 nm and 2400 lines/mm, respectively. The measurements revealed the differences in chemistry of the polymer thin films.

Figure 2 shows the comparative Raman spectra of pPFDA and pHEMA layers in the coated tubes. The large band around 2950 cm^{-1} corresponds to the $\nu_{as}CH_2$ stretching mode [44]. It has been reported that the high region between 2800 and 3100 cm^{-1} includes the Raman bands that are due to valence vibrations of CH_2 and CH_3 [34]. The Raman band at 1454 cm^{-1} demonstrates the deformation of C–H group. The C=C bonds are expected to be deformed during the synthesis process due to the fact that the polymer coatings were deposited inside the tubes by means of free radial polymerization. The band at 1648 cm^{-1} can be attributed to the C=C stretching mode of pPFDA coating. The Raman bands at 1725 and 1740 cm^{-1} correspond to νC=O vibration mode for pHEMA and pPFDA thin film coatings, respectively. (ν: stretching, s: symmetric, as: asymmetric) [44].

In addition, it should be noticed that the band at 2330 cm^{-1} is a noise peak originating from the humid testing environment, not from the samples. It is also found that after performing boiling experiments, there has been no significant change in Raman results for both of the polymer coatings.

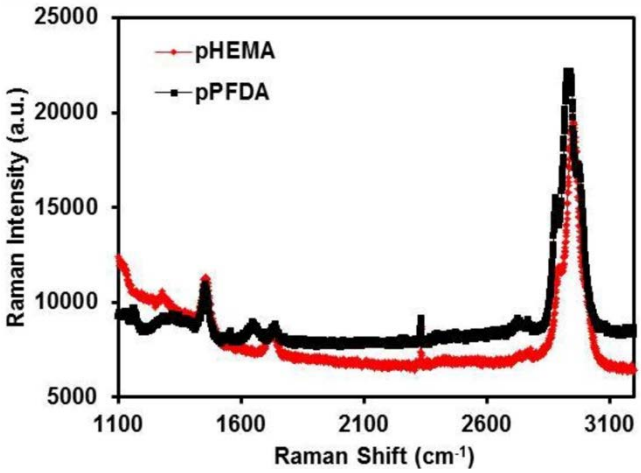

Fig.2. Raman spectrum measured from the inner surface of the coated microtubes

2.2.2 Energy Dispersive Spectra Measurements

Energy Dispersive Spectra (EDS) measurements were used to detect the elemental distribution and chemical characterization of the polymer thin film coatings. As can be observed from Fig. 3, the pHEMA coated part of the microtubes only contains carbon (72.63 wt. %) and oxygen (27.37 wt. %), while pPFDA includes carbon (62.53 wt. %), oxygen (13.42 wt. %) and fluorine (24.05 wt. %). EDS analyses were performed at the Oxford EDS Xmax- N system, which is coupled to the JEOL JIB 4601F MultiBeam platform, using 15keV electron energy and around 30% dead time for signal acquisition.

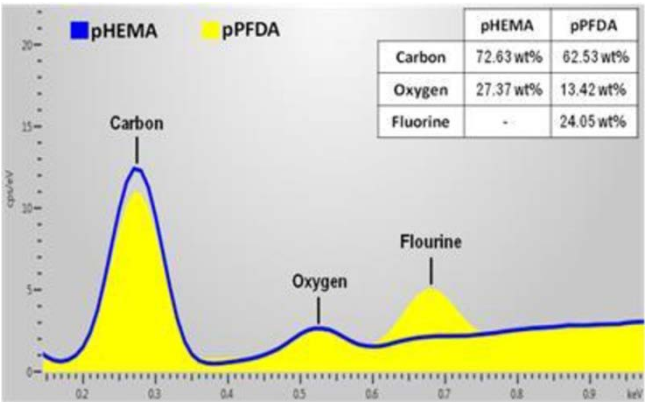

	pHEMA	pPFDA
Carbon	72.63 wt%	62.53 wt%
Oxygen	27.37 wt%	13.42 wt%
Fluorine	-	24.05 wt%

Fig.3. Energy dispersive spectra measurements of the coated microtubes

2.2.3 Contact Angle Measurements

Contact angle measurements were conducted to investigate the hydrophilicity of the surface for different HEMA/PFDA ratios. For these measurements, Si wafers, which were placed next to the microtubes and were coated simultaneously with the same polymer, were used. Figure 4 shows contact angles as a function of the position on Si wafer. It is observed that as going towards the hydrophobic side, the contact angle increases up to 109°, while it reduces to 43° as approaching to the hydrophilic side, confirming the gradient composition of the polymer coating. In the literature, the contact angles of pure pHEMA and pure pPFDA were measured as 37° and 120.8°, respectively [45,46]. The contact angles obtained in this study are within the range reported in the literature.

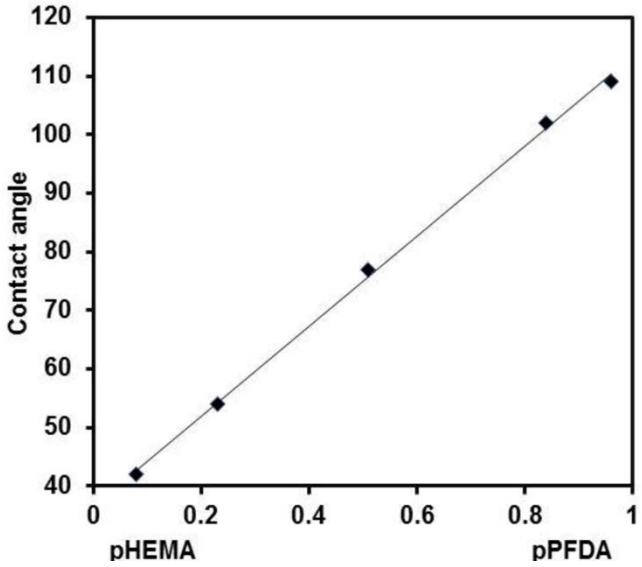

Fig.4. Contact angles between water droplet and coated surface versus position (location/length of the channel)

2.2.4 Scanning Electron Microscopy Images

SEM (Scanning Electron Microscopy) secondary electron (SE) images of the coated microtubes were also acquired using a JEOL JIB 4601F MultiBeam platform (shown in Fig. 1). Figure 5 shows the overall shape of the tubes, surface morphology and the

inner side of the coated tubes. The images were obtained at 5 k eV electron energy for different magnifications from the same microtube.

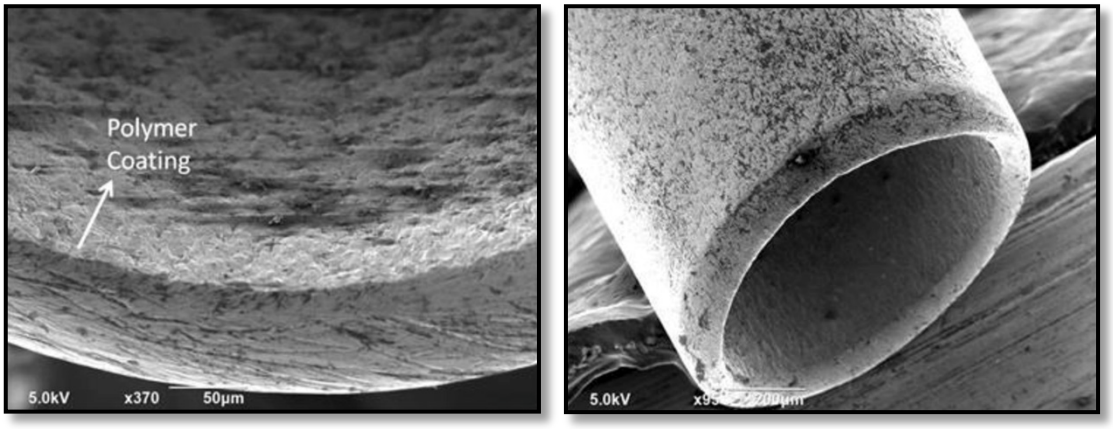

Fig.5. SEM images of the coated microtubes

2.3 Experimental Apparatus and Procedure

The schematic of the experimental setup is shown in Fig. 6. It consisted of a storage cylinder, an Omega® flow meter, a Xantrex XFR2800 power supply, Omega® pressure sensors, thermocouples, a water filter, test section and proper tubing and fittings. De-ionized (DI) water was used as the working fluid in the experiments. Pressurized Nitrogen gas was utilized for pumping the working fluid from the reservoir. A filter of 15 µm sieve diameter was utilized. Two alligator clips, specially shaped with machining tools in order to minimize the heated length and to reach a width of 1 mm, were connected to the microtube surface while adjusting the heated length. The heated length was fixed at 2 cm during the experiments. The high current power supply with an adjustable DC current and high power input provides heating along the heated length to provide the desired heat flux to the prescribed sections of 6 cm long microtubes with inner diameters of 502 µm. The inlet side of the microtube was connected to the setup, while the outlet side was exposed to the atmosphere to attain atmospheric conditions at the exit. One Omega® thermocouple was installed upstream the inlet to measure bulk fluid temperatures at the inlet. Multiple Omega® pressure transducers having different ranges of 0-3000 psi gauge pressure were utilized for pressure measurements. The flow rate data obtained from an Omega® turbinemeter were collected together with the current and voltage data. A thin Omega® thermocouple wire (~76 µm) was carefully

attached on the microtube surface at the desired location via Omega® Bond just at the outlet, where the maximum temperature was expected at the test section, to measure the local surface temperature at the outlet of the tube. During the experiments, the flow rate was fixed at the desired value by regulating the pressure difference between the microtube inlet and exit. Pressure and temperature data were acquired via the Labview® interface after reaching steady state conditions.

Heat loss was calculated by applying power to the test section after evacuating the test section until the temperature of the test section reaches the steady state value. Thereafter, the temperature difference between the test section and ambient was recorded with the corresponding power value so that power against temperature rise profile was obtained. Thus, the heat loss associated with each experimental data point was found with the use of the resulting calibration curve. Accordingly, heat losses were estimated to be about 6% on average. This amount of heat loss is not very significant as expected due to the high flow rates in this study.

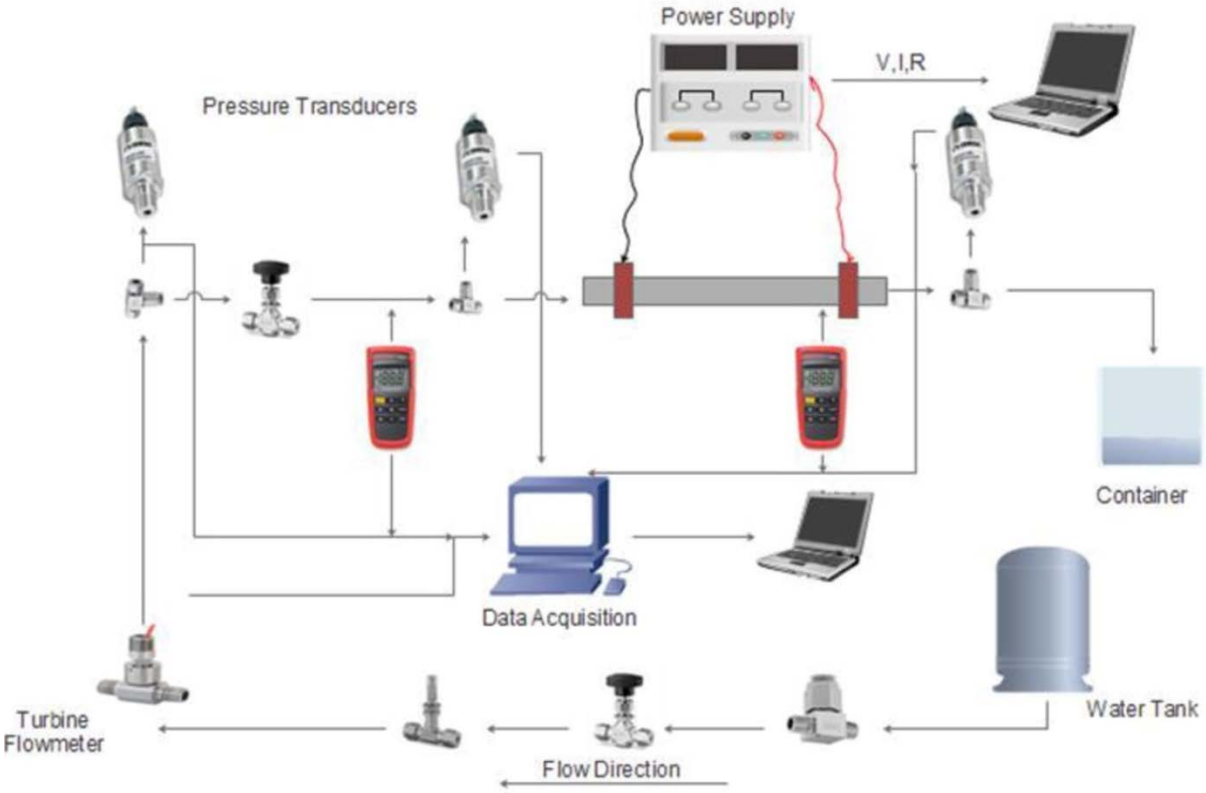

Fig. 6. Schematic of the experimental setup

2.4 Data Reduction and Uncertainties

The collected voltage, current, flow rate, and temperature data are acquired via the Data Acquisition System in order to obtain single-phase and two-phase heat transfer coefficients.

The mass flux, G , is defined as

$$G = \dot{m}/A_c \tag{1}$$

where $\dot{m}$ is the mass flow rate and A_c is the cross section area of the microtube. The applied heat flux is found using the microtube inner diameter and net applied power formula as

$$q'' = \frac{(P - \dot{Q}_{loss})}{\pi d_i L_h} \tag{2}$$

where d_i is the inner diameter of the microtube, L_h is the heated length, and $(P - \dot{Q}_{loss})$ is the applied net power. The heat transfer coefficient at the exit of the tube is expressed as

$$h_{tp} = \frac{(P - \dot{Q}_{loss})}{\pi d_i L_h (T_{w,i} - T_f)} \tag{3}$$

where $T_{w,i}$ is the local inner surface temperature and T_{fluid} is the local bulk fluid temperature at that location. $T_{w,i}$ is calculated using the measured local outer surface temperature,$T_{w,o}$and assuming 1D steady state heat conduction with uniform heat generation as follows

$$T_{w,i} = T_{w,o} + \frac{\dot{q}}{4k_w}(r_o^2 - r_i^2) - \frac{\dot{q}}{2k_w} r_o^2 \log\left(\frac{r_o}{r_i}\right) \tag{4}$$

where r_i and r_o are the inner and outer radii of the microtube, respectively, k_w is the heat thermal conductivity of the wall, and $\dot{q}$ is the volumetric heat generation expressed in terms of the net power as

$$\dot{q} = \frac{(P - \dot{Q}_{loss})}{\pi (r_o^2 - r_i^2) L_h} \tag{5}$$

The local bulk fluid temperature is found via energy balance as

$$T_f = T_i + \left[\frac{(P - \dot{Q}_{loss})x_{th}}{\dot{m}c_p L_h}\right] \quad (6)$$

where $\dot{m}$ is the mass flow rate, c_p is specific heat, T_i is inlet temperature, x_{th} is the thermocouple location, and L_h is the heated length of the microchannel.

Local exit mass quality is calculated using energy balance as

$$x_e = \frac{q''\pi d_i L_h - \dot{m}c_{p,e}(T_{sat,e} - T_i)}{\dot{m}h_{FG,e}} \quad (7)$$

The uncertainties in the measured values are given in Table 1. They are based on the data in the manufacturer's datasheets and the propagation of uncertainty method [47].

TABLE1. Uncertainties in experimental parameters

Parameters	Error
Inner diameter, d_i	± 2 μm
Electrical power, P	± 0.17%
Heat flux, q''	± 3.4%
Two phase heat transfer coefficient, h_{tp}	± 11.8%
Inlet fluid temperature, T	± 0.1^oC
Mass flux, G	± 2.5%

2.5 Results and Discussion

2.5.1 Single phase Validation

Before performing systematic boiling heat transfer experiments on the coated surfaces, single phase tests were performed on plain microtubes in order to check for the validity of the experimental setup. Figure 7 demonstrates experimental results for the plain surface microtube at the mass flux of 9500 kg/m^{2}s. Since turbulent flow conditions existed (7000<Re<11000), the results were compared to the two well-known empirical correlations recommended for turbulent flows: Dittus-Boelter and Gnielinski correlations as shown in Eqs (8) and (9) respectively [48]:

$$Nu = 0.023\, Re^{0.8}\, Pr^{0.4} \quad (8)$$

$$Nu = \frac{\left(\frac{f}{8}\right)(Re-1000)Pr}{1+12.7\,(f/8)^{0.5}\,(Pr^{\frac{2}{3}}-1)} \quad (9)$$

The following expression [42] was used to calculate f (friction factor) in Eq. (9):

$$f = (0.79\ln Re - 1.69)^{-2} \quad (10)$$

A good agreement can be observed between the experimental results and the predictions of the two correlations. The maximum errors corresponding to Dittus-Boelter and Gnielinski correlations were about 12% and 15%, respectively. In this study, axial conduction effects were considered to be negligible due to high mass flux in this study that results in high Peclet number (ranging from about 30377 to 31974) which is defined as the product of the Reynolds number and the Prantdl number [49,50].

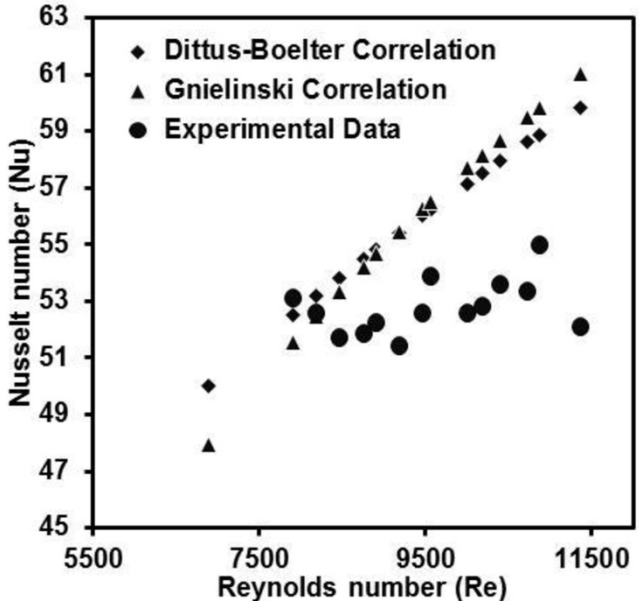

Fig.7. Experimental results for single phase in comparison with the existing correlations

2.5.2 Boiling curves

In order to investigate effects of the variations in wettability, experiments were conducted in two directions of the microtubes such that first the hydrophilic inlet

(pHEMA coated inlet) and the hydrophobic outlet (pPFDA coated outlet) were considered. The tests were then repeated for the opposite case (pPFDA coated inlet and pHEMA coated outlet). Figure 8 displaying the boiling curves for the coated tubes at the mass flux of 9500 kg/m^{2}s illustrates that coated tubes result in a lower wall superheat at a fixed heat flux relative to the bare surface tube. Therefore, a shift to the left can be seen for the coated tubes, and the highest shift occurs in the microtube with the pHEMA coated (hydrophilic outlet) outlet. This is due to the decreased contact angle of the pHEMA coated side. Contact angle measurements revealed that the wettability varied from about 40 º to about 110 º when moving along the microtube from the pHEMA coated side to the pPFDA coated side. Therefore, higher heat fluxes could be sustained by the extra wetting layer on the inner walls of the microtube near the outlet.

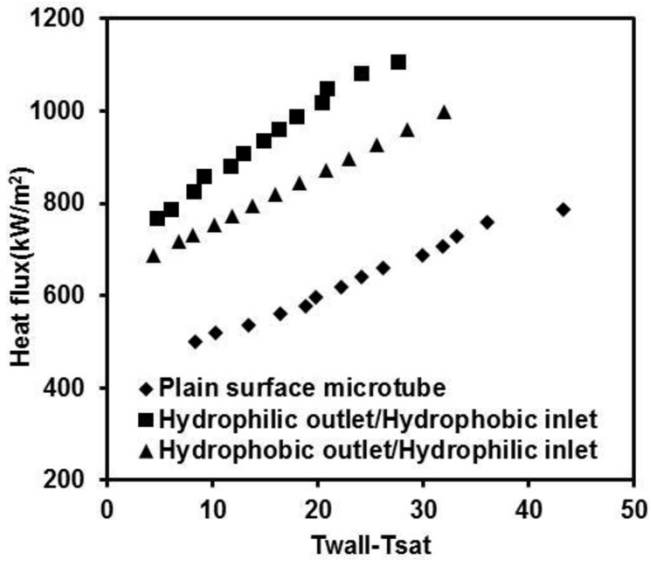

Fig.8. Boiling curves related to bare surface microtubes and gradient coated microtubes

Figure 9 illustrates outlet local vapor quality as a function of heat transfer coefficient. As it can be seen, as vapor quality increases, heat transfer coefficient increases. This can be associated to the produced more active nucleation sites which promote nucleate boiling and leads to better heat transfer performance.

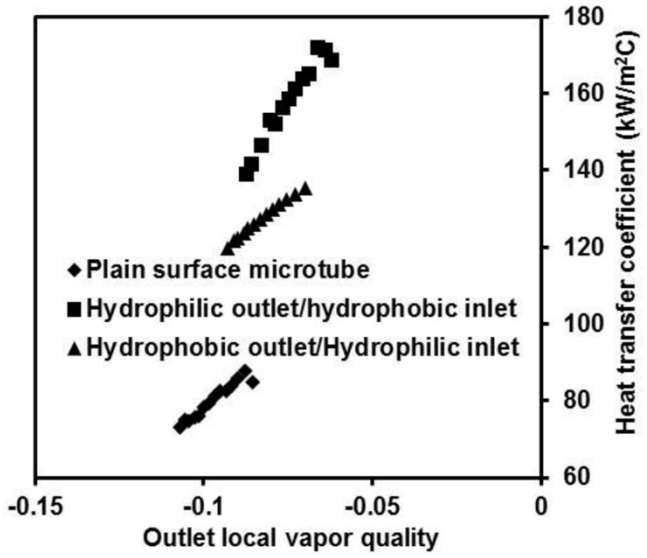

Fig.9. Vapor quality versus heat transfer coefficient

2.5.3 Heat Transfer Results

Figure 10 displays experimental boiling heat transfer coefficients as a function of heat flux. It is obvious from the figure that heat transfer is significantly enhanced with gradient pHEMA/pPFDA coatings. At high heat fluxes, heat transfer coefficients have higher values for all the experiments, which is associated with more nucleation at higher heat fluxes. Enhanced heat transfer in coated microtubes is due to the high porosity of the surface, which enables more nucleation and quicker bubble release from the surface. For the pHEMA coated inlet and pPFDA coated outlet (hydrophilic outlet and hydrophobic inlet), this effect is more dominant near the inlet of the heated section, while it is more pronounced toward the outlet for the hydrophobic outlet (pPFDA coated outlet, pHEMA coated inlet). The configuration with the pHEMA coated outlet benefits from the more hydrophilic surface near the outlet, where the surface temperature is expected to be the highest. This location is therefore more critical for the formation of dry spots, which badly influence heat transfer. More wettability toward the outlet facilitates rewetting of the surface thereby avoiding deterioration in heat transfer. For the configuration with the pPFDA coated outlet and pHEMA coated inlet (hydrophobic outlet, hydrophilic inlet), the locations near the outlet are more hydrophobic. At these critical locations, rewetting becomes more difficult. As a result, dry spots are more likely to appear on the surface for these coatings, which results in a worse performance than the case with the hydrophilic outlet and hydrophobic inlet.

Another feature of the coatings is offering variations in wettability along the microtube. The existence of wettability gradient mitigates liquid motion and bubble motion near the surface thereby enhancing convective heat transfer. Positive effects of wettability gradient were also documented in the literature on heat and mass transfer in micro scale [51–53]. The maximum heat transfer enhancement ratios were about 64% and 47% for the configurations with the pHEMA and pPFDA coated outlets (hydrophilic outlet/hydrophobic inlet and hydrophobic outlet/hydrophilic inlet), respectively. The higher enhancements compared to the previous study of the authors (a reported enhancement of 26% in Kaya et al. [34]) on microtubes of the similar size are a clear evidence of enhanced convective effects and mitigation of bubble motion with the variation in wettability.

The experimental results obtained in this study revealed that the use of pHEMA and pPFDA coatings, which provide variations in wettability along the channel, could be a viable alternative for a superior boiling heat transfer performance. However, more studies are needed to investigate different parameters of these types of coatings to optimize the heat transfer performance of such enhancement techniques.

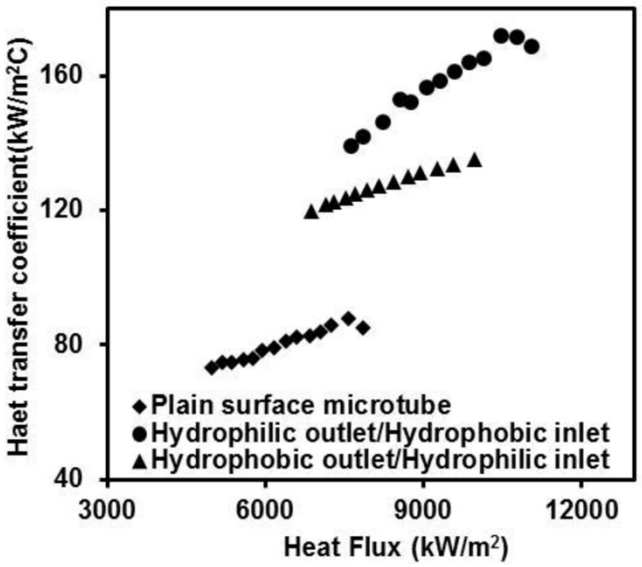

Fig.10. Boiling heat transfer coefficients versus heat flux profiles

CHAPTER 3

Investigation of Subcooled Flow Boiling Heat Transfer using Hierarchically Structured Plates Integrated into a Rectangular Microchannel

3.1 Sample Preparation

In our two-phase heat transfer experiments, Al alloy 2024 surfaces with both super hydrophobic (SHP) and oleophobic properties were utilized. The reason for utilizing this material was the extensive use of Al alloy in industry due to its light weight and mechanical robustness. When combined with SHP and oleophobic properties, it can be implemented in a wide range of industrial applications [54,55]. Two simple, industrially scalable, and environmentally friendly techniques were used to construct such surfaces, namely: 1) randomly mechanical sanding; 2) post treatment in boiling DI water for 1 minute. The schematic representation of the preparation procedure is shown in Fig.11. As seen in the figure, the major steps for the preparation of such surfaces were as follows: First, the plates were randomly sanded using sandpapers of different grit sizes of 36, 60, 400, and 1000 for 20 seconds with an applied pressure of 3.0 ± 0.2 kg/cm^2 to construct micro structures. The micro structured plates were submerged into boiling DI water for 1 min. to introduce the nanograss layer. The micro and nano structured plates were ultrasonicated with acetone, isopropanol, and DI water for 10 min. each and then cleaned with nitrogen gas. To decrease the surface energy of the roughened plates, 5% perfluorodecyltriethoxysilane (PFDTS) solution of toluene along with the micro and nanostructured plates were put in a sealed bottle inside an oven at 90ºC for 3 hours. Finally, the chemically altered roughened surfaces were put in an ambient environment for more than 12 hours to be entirely dried [56].

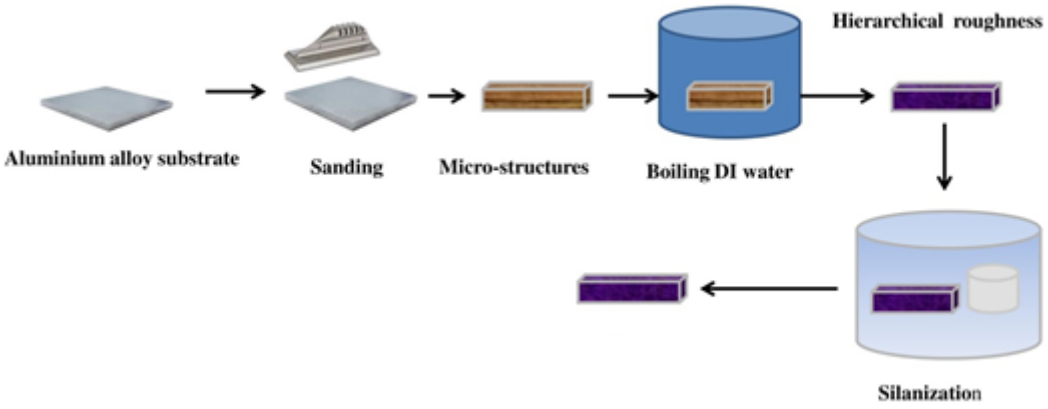

Fig.11. Schematic illustration of preparation process of micro and nano structured plates

Characterization of the surfaces of the final products of aforementioned process was performed by using Scanning Electron Microscopy (SEM, JEOL 7000F) as shown in Figs. 12a-e. Figure 12e illustrates a higher magnification image of the plate sanded with sandpaper of grit size 36. As shown in Fig. 12e, the micro-structures are uniformly covered with the nanograss layer.

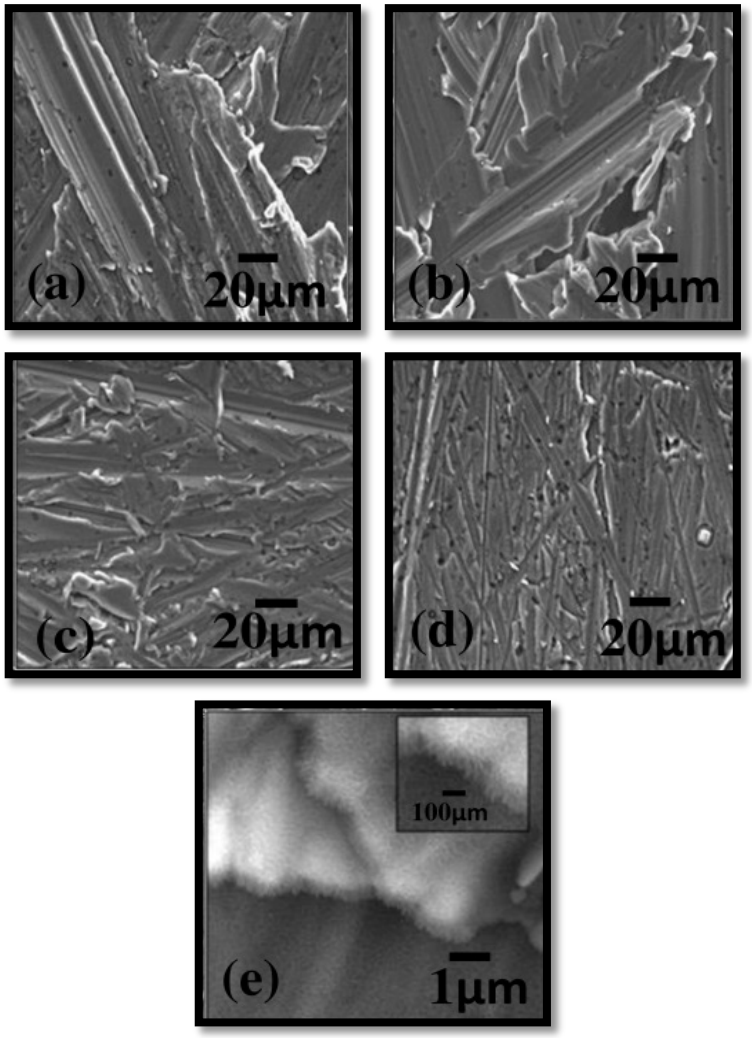

Fig.12. SEM images of micro and nanostructured surfaces sanded with grit sizes of a) 36; b) 60; c) 400; d) 1000; and e) high magnification SEM image for the surface roughened with grit size 36

Figure 13 illustrates contact angles corresponding to the hierarchically roughened surfaces with sandpapers at grit sizes ranging from 36 to 1000, which were measured using a VCA Optima goniometer. From the figure, it can be understood that the samples have super hydrophobic and oleophobic properties.

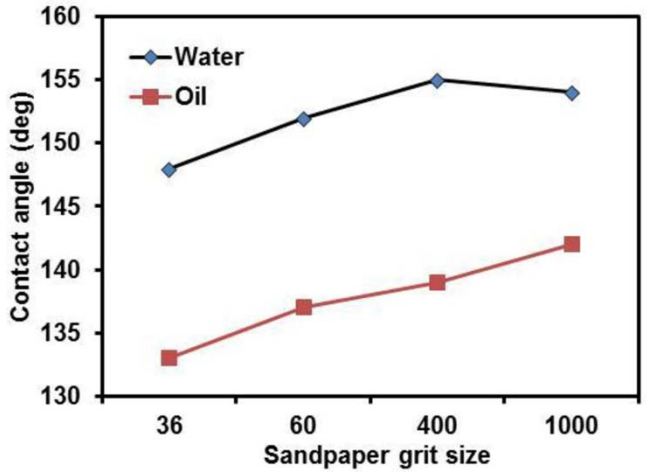

Fig.13. Contact angles of micro and nano structured surfaces sanded with different grit sizes of 36, 60, 400, and 1000 for both water and oil

3.2 Experimental Setup and Procedure

The schematic of the experimental setup is shown in Fig. 14. The setup included a storage container, an Omega® pressure sensor, four Omega® cartridge heaters, an MZR®-7205 micro annular gear pump, UNI-T UT325 thermometers, four K-type Omega® thermocouples, an AMETEK Sorensen XHR DC regulated power supply, test section , proper tubing and fittings. Deionized water (DI) was used as the working liquid. DI water was pumped into the microchannel using the micro gear pump. Mass fluxes were regulated by the micro pump's own controller.

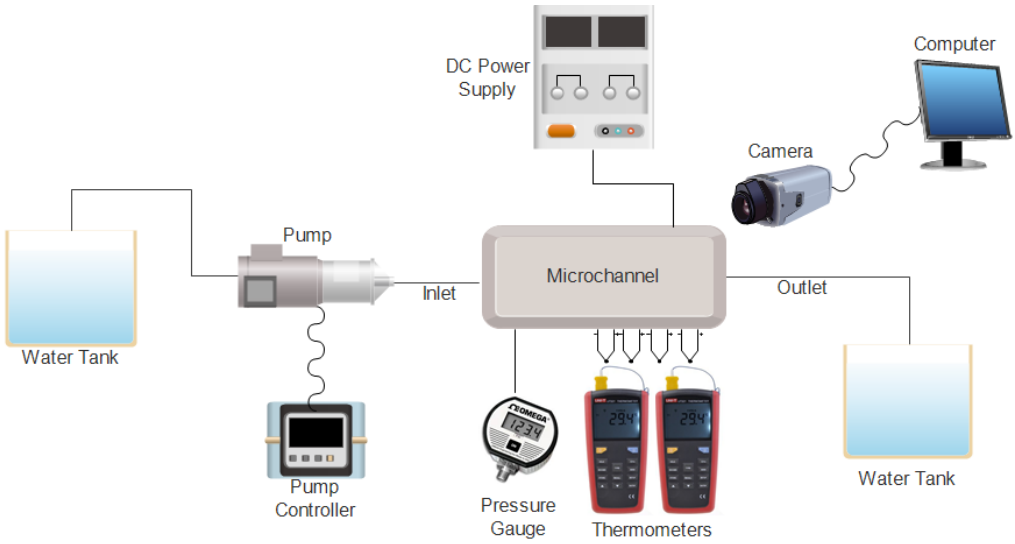

Fig.14. Schematic representation of the experimental setup

Fig. 15 shows the schematic representation of the experimental test section. The Al channel had a length, width, and depth of 14 cm, 1.5 cm, and 500 µm, respectively. Four cylindrical cartridge heaters, each having a diameter of 7.5 mm, were attached to the grooves under the microchannel to supply heat flux by applying voltage. The cartridge heaters, spaced approximately 0.25 mm from each other, were connected in parallel. Surface temperatures were measured using four K-Type Omega® thermocouples, each having a diameter of 3 mm, which were connected to the digital thermometers. A square hole of 150×150 mm was built inside the microchannel near the exit to embed the micro and nanostructure plates via high quality thermal grease. The inlet pressure of the channel was measured using a pressure gauge at the inlet port, while the outlet was subjected to the atmosphere. The upper side of the microchannel was covered by a Plexiglas plate to enable flow visualization. In order to minimize heat losses, 4 mm wide air gaps were located between the heaters to enclose the heaters with air from all sides.

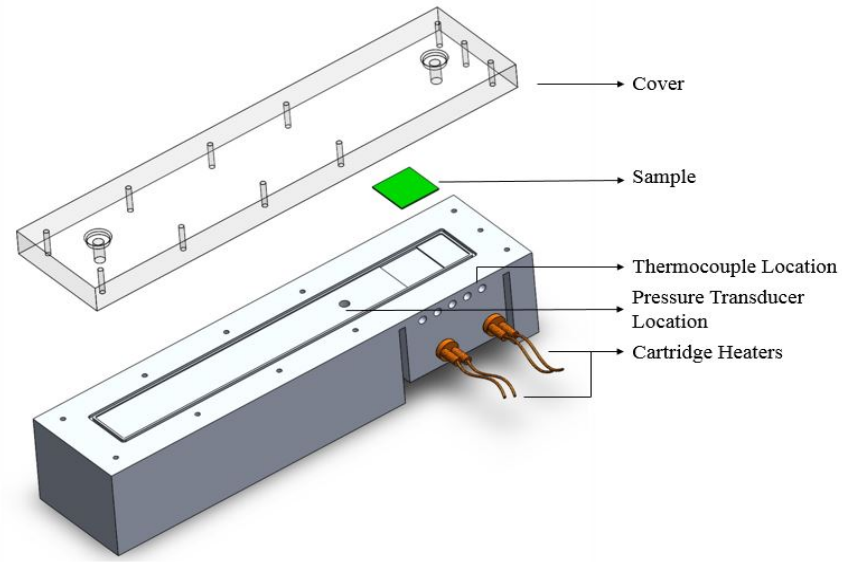

Fig.15. Schematic illustration of the experimental test section

Heat losses were calculated based on natural convection analysis as follows

$$\dot{Q}_{loss} = hA_s(T_s - T_{amb}) \tag{11}$$

where A_s is the surface area of the plate, T_{amb} is ambient temperature, and h is the natural convective heat transfer coefficient.

3.3 Data Reduction and Uncertainties

Data collected from voltage, current, temperature, and flow rate measurements were used to calculate two phase heat transfer coefficients.

The heat flux, q'', is defined as

$$q'' = \frac{(P - \dot{Q}_{loss})}{A} \tag{12}$$

where $(P - \dot{Q}_{loss})$ represents the applied net power and A is the heated surface area. The surface temperatures of the microchannel, T_s, were calculated by considering thermal contact resistances from the thermocouples to the surface of the micro and nanostructured plate as

$$T_s = T_{th} - q''R_{tot} \quad (13)$$

where T_{th} is the thermocouple temperature reading of the thermometer and R_{tot} is the total thermal resistance calculated by considering the thermal resistance of the grease at the interface between the Al base and the micro and nanostructured plate, R_{tg} and the resistance of the plate, R_{plate} as

$$R_{tot} = R_{tg} + R_{plate} \quad (14)$$

The heat transfer coefficient is expressed as

$$h = \frac{q''}{T_s - T_f} \quad (15)$$

where T_s is the surface temperature and T_f is the local bulk fluid temperature which is given as

$$T_f = T_i + \left[\frac{(P - Q_{loss})x_{th}}{\dot{m}c_p L_h}\right] \quad (16)$$

where T_i is the inlet fluid temperature, $\dot{m}$ is the mass flow rate, c_p is specific heat of water, x_{th} is thermocouple location, and L_h is the heated length. The Nusselt number for the single phase data is obtained from

$$Nu = \frac{hD_h}{k} \quad (17)$$

where D_h is the hydraulic diameter of the channel and k is the thermal conductivity of water. The flow velocity, u, is expressed as

$$u = \frac{\dot{Q}}{A_c} \quad (18)$$

where $\dot{Q}$ is the volumetric flow rate of water and A_c is the cross sectional area of the channel. The Reynolds number, Re, is given as

$$Re = \frac{\rho u D_h}{\mu} \quad (19)$$

where μ is the water dynamic viscosity. The single phase friction factor was calculated using

$$f = (0.79\ln(Re) - 1.64)^{-2} \quad (20)$$

The uncertainties in the measured parameters are shown in Table 2. The uncertainties were calculated according to manufacturers' datasheets and the propagation of uncertainty method presented by Kline and McClintock [47].

Table2. Uncertainties of the experimental parameters

Parameters	Uncertainty
Power, P	± 0.15 %
Heat transfer coefficient, h	± 8.4 %
Heat flux, $\mathbf{q''}$	± 3.5 %
Volumetric flow rate, $\dot{\mathbf{Q}}$	± 1 %
Thermocouple temperature, $\mathbf{T_{th}}$	± 0.1 ºC
Surface temperature, $\mathbf{T_s}$	± 0.37 ºC
Thermal resistance, $\mathbf{R_{tot}}$	± 5 %

3.4 Results and Discussion

3.4.1 Single phase Validation

To validate the experimental setup, single phase tests were initially carried out using an untreated Al alloy plate. The experimental Nusselt numbers and friction factors were compared to the predictions of Gnielinski (Eq. 9) and Blasius (Eq. 21) correlations, respectively, which were suggested for turbulent flows as plotted in Fig. 16. As seen from the figure, experimental Nusselt numbers and friction factors demonstrated a notable agreement with the results obtained from available correlations. (Maximum errors related to Nusselt number and friction factor were ~ 30% and ~ 5%, respectively.)

$$f = \frac{0.316}{Re^{-1/4}} \tag{21}$$

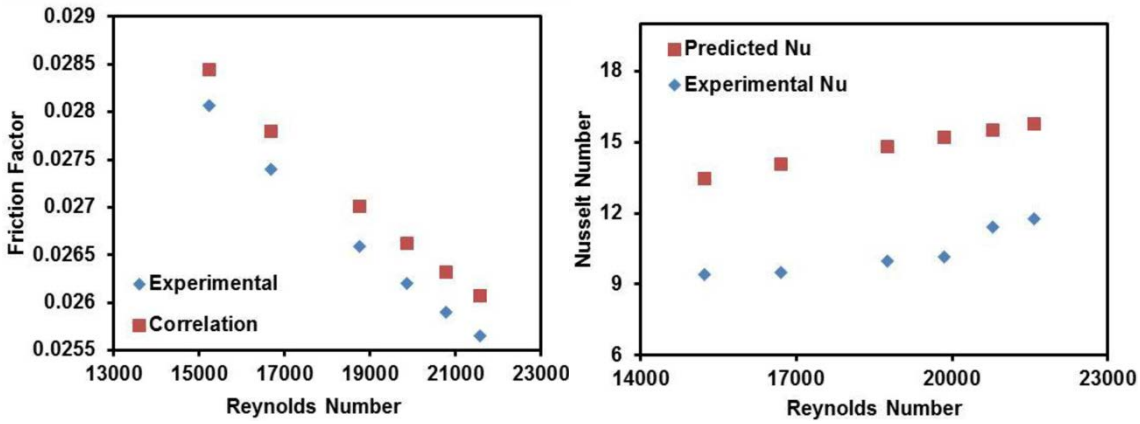

Fig.16. Comparison of the experimental single phase Nusselt number and friction factor corresponding to the untreated plate with the predictions of available correlations

3.4.2 Flow Boiling Curves

Figures 17 (a-c) demonstrate local wall temperatures as a function of heat flux for micro and nano structured plates sanded using sandpapers of different grit sizes of 36, 60, 400, and 1000 and the untreated plate at three mass fluxes of 75, 100, and 125 kg/m^{2}s. As seen from Fig. 17a, the wall temperature increases with heat flux. The wall temperatures of the plates sanded with sandpapers of grit sizes of 36 and 60 are greater than those with grit sizes of 400 and 1000, and even the untreated plate. The higher wall temperature obtained from the surfaces roughened with grit sizes of 36 and 60 compared to the untreated one as well as to other surfaces can be associated with a low number of active nucleation sites. Similar observations can be made at higher mass fluxes (Figs. 17b and 17c). With an increase in mass flux, the wall temperature decreases due to bubble motions with higher velocities and a greater number of active nucleation sites, as observed in the flow visualization results, which will be covered later in the thesis.

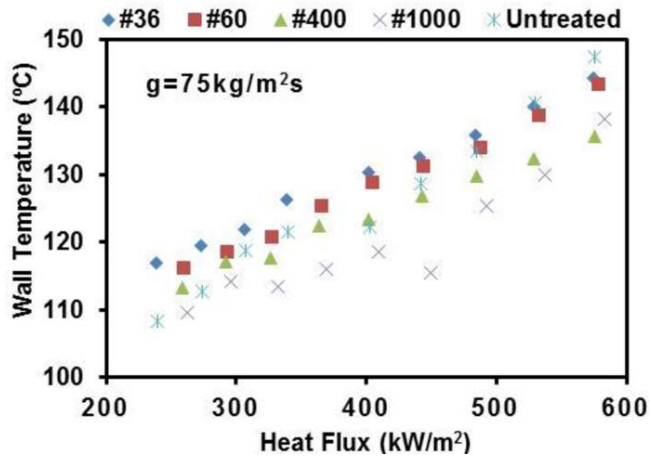

(a)

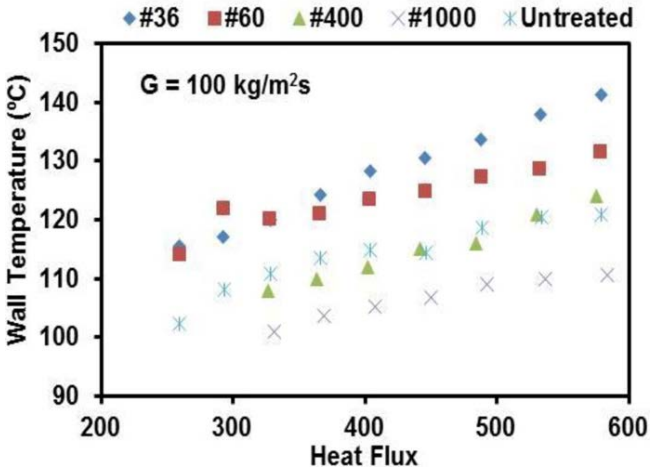

(b)

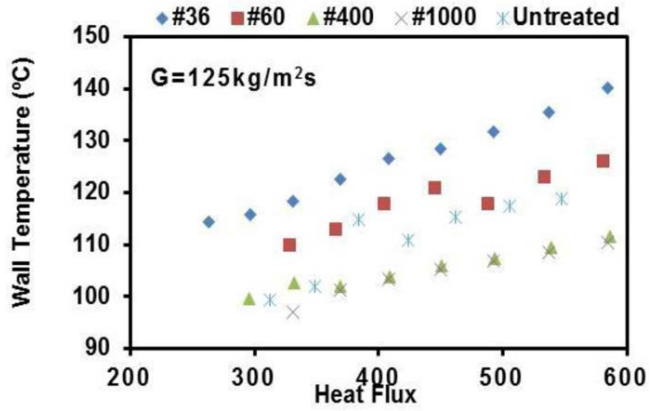

(c)

Fig.17. Wall temperature of micro and nano structured plates sanded with sandpapers of grit sizes ranging from 36 to 1000 and the untreated plate as a function of heat flux at different mass fluxes of a) G=75; b) G=100; and c) G=125 kg/m^{2}s

The local heat transfer coefficients are presented as a function of heat flux in Fig. 18 for different micro and nano structured plates and mass fluxes. The local heat transfer coefficients corresponding to the middle of the plates were taken into consideration. The surfaces roughened using sandpapers with grit sizes of 400 and 1000 led to higher heat transfer coefficients compared to those sanded with grit sizes of 36 and 60 and the untreated surface. It is also noticeable that heat transfer coefficients related to surfaces roughened with grit sizes of 36 and 60 are lower than those of the untreated surface. This deterioration has already been reported in the literature [11,57–59]. For example, Ramilson et al. [57] reported that the surface-liquid interaction effect is a significant factor in determining heat transfer coefficient (HTC) on both rough and smooth surfaces. Berenson [59] found heat transfer coefficient more pertinent to a lapped surface than to a roughened surface. In addition, the method of roughening surfaces either by machining or sanding with sandpapers in different grit sizes can lead to different results [60]. The poor performance of the surfaces sanded with grits of 36 and 60 with respect to the untreated plate may be due to the microstructures and nanograss made in the fabrication process, which results in a decrease in wetting area and nucleation site densities, and also in the possibility of the vapor being trapped in the cavities under the experimental conditions. The higher HTC observed in the surfaces sanded with grits of 400 and 1000 can be associated with the enlarged and faster bubbles during boiling, a greater number of active nucleation sites, and increase in heat transfer surface area. Maximum enhancement corresponding to the plates sanded with grits of 400 and 1000 was found to be about 25% and 42%, respectively, at heat flux of about 408 kW/m^2 and mass flux of G=125 kg/m^{2}s. It can be observed that similar trends are present for the local heat transfer coefficients at other mass fluxes.

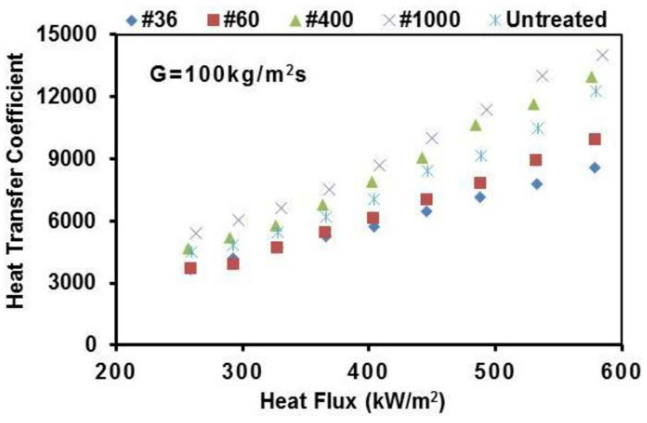

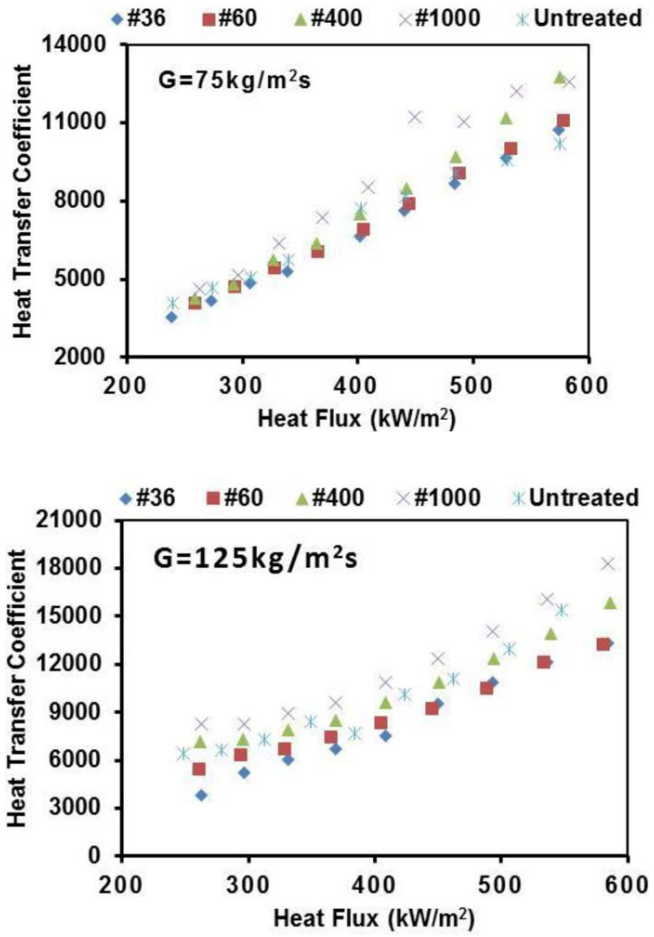

Fig.18. Heat transfer coefficients of micro and nano structured plates sanded with sandpapers of grit sizes ranging from 36 to 1000 and the untreated plate as a function of heat flux at different mass fluxes

The wall superheat, defined as the temperature difference between the wall temperature and the saturation temperature, versus heat flux at three different mass fluxes was plotted in Fig. 19. As seen from the boiling curves, the micro and nano structured plates sanded with grit sizes of 400 and 1000 had lower wall superheat at a fixed heat flux. At mass fluxes of 100 and 125 kg/m^{2}s, hierarchical plates sanded with grit sizes of 400 and 1000 had nearly the same wall superheat implying saturation in the results based on grit size.

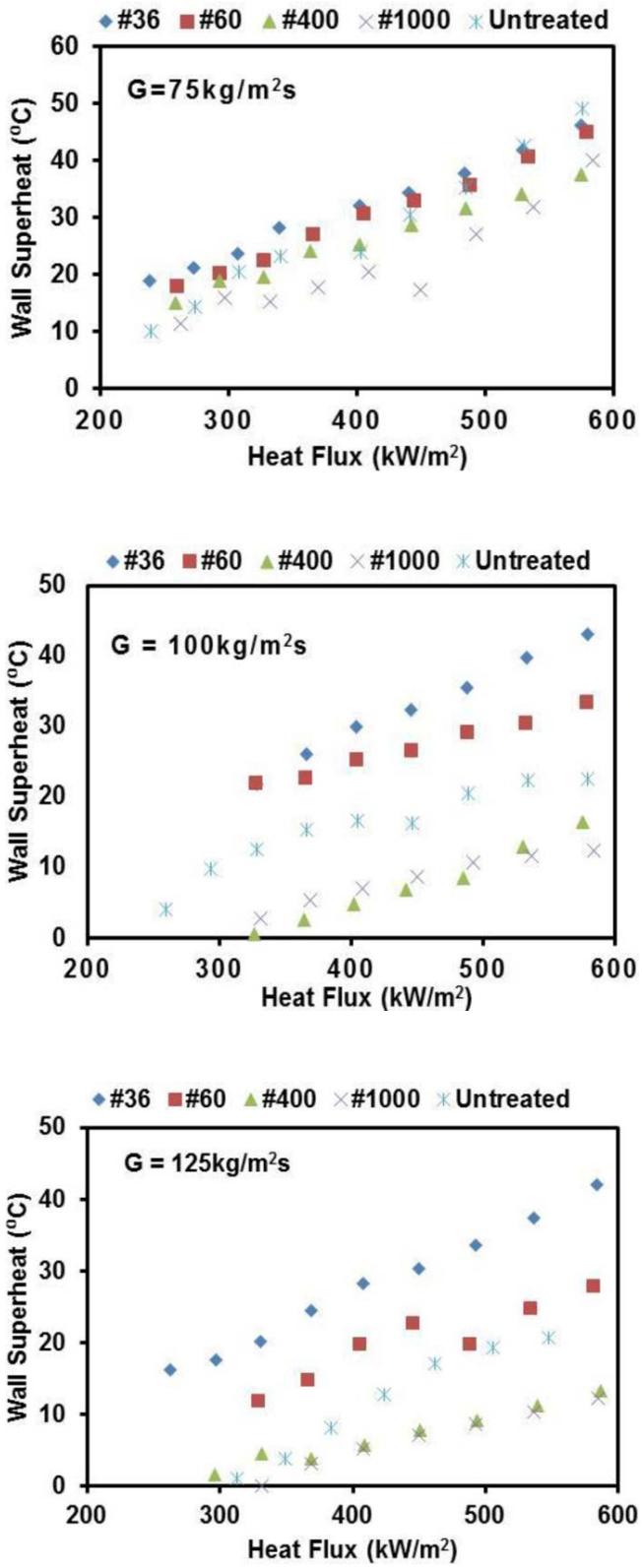

Fig.19. Wall superheat in micro and nano structured plates sanded with sandpapers in grit sizes ranging from 36 to 1000 and the untreated plate as a function of heat flux at different mass fluxes

3.4.3 Flow Visualization

Figure 20 illustrates flow boiling images on Al alloy micro and nanostructured plates sanded with various grit sizes of 36, 60, 400, and 1000 as well as the untreated plate. In the figure related to the untreated plate, we can see that a lower number of discrete bubbles emerged and then slid over the heating surface. For the surfaces sanded with grit sizes of 36 and 60, smaller bubbles appeared and moved with a smaller velocity, and no coalescence of bubbles occurred.

For the surfaces sanded with grit sizes of 400 and 1000, a larger number of bubbles was produced and bubble sizes became large with coalescence of bubbles forming the vapor slugs, which also moved with a higher velocity. Different boiling flow patterns related to the surfaces sanded with grit sizes of 400 and 1000 compared to the other surfaces lead to a significant enhancement in boiling heat transfer with these plates.

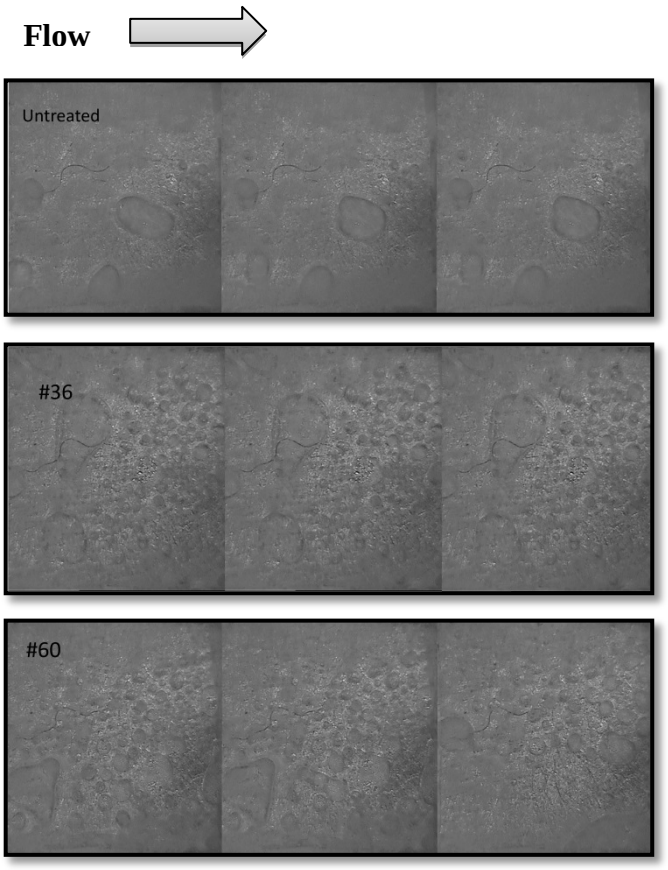

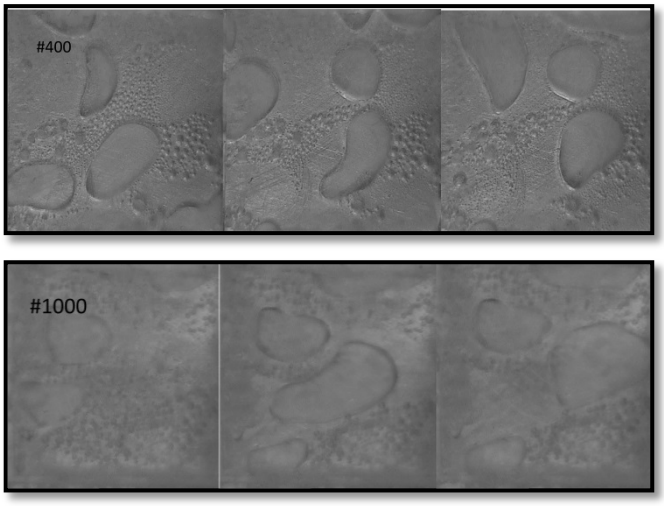

Fig.20. Flow boiling images related to the micro and nanostructured surfaces sanded with different grit sizes and the untreated plate

CHAPTER 4

CONCLUSIONS AND FUTURE WORK

4.1 Conclusions

In this thesis, subcooled flow boiling heat transfer was first investigated in the microtubes with gradient poly hydroxyethyl methacrylate (pHEMA) and poly perfluorodecylacrylate (pPFDA) coatings, which offered variations in wettability along the microtube (increase and decrease toward the outlet, respectively). The main findings are as follows:

1. Gradient pHEMA/pPFDA coated microtubes offered superior boiling heat transfer performances in comparison to the plain surface microtube due to more active nucleation sites which yields in higher nucleation site densities, bubble generation frequency of the surface, as well as enhanced convective effects with the variation in wettability and improved liquid replenishment after bubble departure.
2. The best heat transfer coefficients corresponded to the configuration with the hydrophilic outlet and hydrophobic inlet (pHEMA coated outlet, pPFDA coated inlet) due to the higher wettability at critical locations and more active nucleation sites near the inlet. The maximum enhancement ratio in this configuration was ~64% while it was ~47% for the configuration with the hydrophilic inlet and hydrophobic outlet (pHEMA coated inlet, pPFDA coated outlet) at the same heat flux.
3. iCVD method was utilized for coating the inner walls of the microtubes. The results revealed that iCVD is an advantageous technique for having functional coatings on microchannel/tube surfaces with closed cross section geometries, where the application of existing conventional fabrication methods is limited.

In the second study, subcooled flow boiling experiments were carried out using different micro and nano structured plates integrated into a rectangular aluminum microchannel. The micro and nano structured plates were fabricated by environmentally friendly and simple techniques. The experiments were conducted using deionized water for three mass fluxes of 75, 100, and 125 kg/m^{2}s and the results were compared to each other and to the untreated plate. A high speed camera was mounted on top of the microchannel for visualizing flow patterns during the boiling experiments. Major conclusions drawn from the results are as follows:

- The local heat transfer coefficients of the micro and nano structure plates sanded with grit sizes of 400 and 1000 were higher with enhancement ratios of ~ 25% and ~ 42%, respectively, at mass flux of 125 kg/m^{2}s and heat flux of ~ 408 kW/m^2. This can be associated with enlarged and faster bubble movement and also increase in the heating surface area, which resulted in the lower wall superheats in boiling curves at a fixed heat flux.
- Plates sanded with grit sizes of 36 and 60 represented deterioration in heat transfer coefficients than those of the untreated plate owing to a low number of active nucleation sites and a decrease in the wetted surface area.
- Experimental results were supported by visualization studies on micro and nano structured plates and the untreated plate.
- Experimental results revealed that micro and nano structured plates could enhance boiling heat transfer using environmentally friendly techniques such as sanding and then boiling in DI water and could be easily implemented in heating and cooling applications.

4.2 Future Work

Based on the studies performed in this thesis, the following subjects will be considered as future work:

- For the studies related to the microtubes enhanced by pHEMA/pPFDA coatings:

1) The microtubes with different inner diameters will be studied to investigate the effects of diameter on subcooled boiling heat transfer with enhanced microtubes.
2) Various mass fluxes will be considered to investigate the effects of mass flux on the heat transfer performance with the coated tubes.
3) Different working fluids will be tested to study the cooling performance of the coated microtubes with various fluids.

- For the study related to the micro and nanostructured plates integrated into a microchannel:

1) Microchannels with different structures will be used to study the effects of different geometries on subcooled boiling heat transfer with micro and nanostructured plates.
2) The experiments will be performed using different working fluids.

References

[1] S.P. Sukhatme, A Textbook on Heat Transfer, Universities Press, 2005.

[2] T.L. Bergman, A.S. Lavine, F.P. Incropera, D.P. DeWitt, Fundamentals of Heat and Mass Transfer, 2011.

[3] L.S. Tong, Y.S. Tang, Boiling Heat Transfer And Two-Phase Flow, CRC Press, 1997.

[4] N.-T. Nguyen, S.T. Wereley, Fundamentals and Applications of Microfluidics, Artech House, 2002.

[5] T. Nguyen, M. Mochizuki, K. Mashiko, Y. Saito, I. Sauciuc, Use of heat pipe/heat sink for thermal management of high performance CPUs, in: Sixt. Annu. IEEE Semicond. Therm. Meas. Manag. Symp. (Cat. No.00CH37068), IEEE, 2000: pp. 76–79.

[6] J.C. Chen, Convective Flow Boiling, CRC Press, 1996.

[7] D.J. Beebe, G.A. Mensing, G.M. Walker, Physics and applications of microfluidics in biology., Annu. Rev. Biomed. Eng. 4 (2002) 261–86.

[8] D.B. Weibel, G.M. Whitesides, Applications of microfluidics in chemical biology., Curr. Opin. Chem. Biol. 10 (2006) 584–91.

[9] S.A. Mousavi Shaegh, N.-T. Nguyen, S.H. Chan, A review on membraneless laminar flow-based fuel cells, Int. J. Hydrogen Energy. 36 (2011) 5675–5694.

[10] B. Ziaie, Hard and soft micromachining for BioMEMS: review of techniques and examples of applications in microfluidics and drug delivery, Adv. Drug Deliv. Rev. 56 (2004) 145–172.

[11] P.J. Berenson, Experiments on pool-boiling heat transfer, Int. J. Heat Mass Transf. 5 (1962) 985–999.

[12] R.J. Benjamin, A.R. Balakrishnan, Nucleation site density in pool boiling of saturated pure liquids: Effect of surface microroughness and surface and liquid physical properties, Exp. Therm. Fluid Sci. 15 (1997) 32–42.

[13] M.-G. Kang, Effect of surface roughness on pool boiling heat transfer, Int. J. Heat Mass Transf. 43 (2000) 4073–4085.

[14] J.-Y. Jung, H.-Y. Kwak, Effect of surface condition on boiling heat transfer from silicon chip with submicron-scale roughness, Int. J. Heat Mass Transf. 49 (2006) 4543–4551.

[15] T. Alam, P.S. Lee, C.R. Yap, Effects of surface roughness on flow boiling in silicon microgap heat sinks, Int. J. Heat Mass Transf. 64 (2013) 28–41.

[16] W. Wu, H. Bostanci, L.C. Chow, Y. Hong, M. Su, J.P. Kizito, Nucleate boiling heat transfer enhancement for water and FC-72 on titanium oxide and silicon oxide surfaces, Int. J. Heat Mass Transf. 53 (2010) 1773–1777.

[17] J.P. McHale, S. V. Garimella, Bubble nucleation characteristics in pool boiling of a wetting liquid on smooth and rough surfaces, Int. J. Multiph. Flow. 36 (2010) 249–260.

[18] C.N. Ammerman, S.M. You, Enhancing Small-Channel Convective Boiling Performance Using a Microporous Surface Coating, J. Heat Transfer. 123 (2001) 976.

[19] C. Young Lee, M.M. Hossain Bhuiya, K.J. Kim, Pool boiling heat transfer with nano-porous surface, Int. J. Heat Mass Transf. 53 (2010) 4274–4279.

[20] M. Gulliksen, H. Haugerud, H. Kristiansen, Enhanced boiling heat transfer with porous silver coatings for electronics cooling, Proc. 5th ASME/JSME Jt. Therm. Eng. Conf. (1999) 15–19.

[21] M.S. Sarwar, Y.H. Jeong, S.H. Chang, Subcooled flow boiling CHF enhancement with porous surface coatings, Int. J. Heat Mass Transf. 50 (2007) 3649–3657.

[22] Y. Sun, L. Zhang, H. Xu, X. Zhong, Flow boiling enhancement of FC-72 from microporous surfaces in minichannels, Exp. Therm. Fluid Sci. 35 (2011) 1418–1426.

[23] Y. Sun, L. Zhang, H. Xu, X. Zhong, Subcooled flow boiling heat transfer from microporous surfaces in a small channel, Int. J. Therm. Sci. 50 (2011) 881–889.

[24] H.T. Phan, N. Caney, P. Marty, S. Colasson, J. Gavillet, Surface wettability control by nanocoating: The effects on pool boiling heat transfer and nucleation mechanism, Int. J. Heat Mass Transf. 52 (2009) 5459–5471.

[25] T.J. Hendricks, S. Krishnan, C. Choi, C.-H. Chang, B. Paul, Enhancement of pool-boiling heat transfer using nanostructured surfaces on aluminum and copper, Int. J. Heat Mass Transf. 53 (2010) 3357–3365.

[26] E. Forrest, E. Williamson, J. Buongiorno, L.-W. Hu, M. Rubner, R. Cohen, Augmentation of nucleate boiling heat transfer and critical heat flux using nanoparticle thin-film coatings, Int. J. Heat Mass Transf. 53 (2010) 58–67.

[27] B. Stutz, C.H.S. Morceli, M.D.F. da Silva, S. Cioulachtjian, J. Bonjour, Influence of nanoparticle surface coating on pool boiling, Exp. Therm. Fluid Sci. 35 (2011) 1239–1249.

[28] A.K.M.M. Morshed, T.C. Paul, J. Khan, Effect of Cu–Al2O3 nanocomposite coating on flow boiling performance of a microchannel, Appl. Therm. Eng. 51 (2013) 1135–1143.

[29] V. Khanikar, I. Mudawar, T. Fisher, Effects of carbon nanotube coating on flow boiling in a micro-channel, Int. J. Heat Mass Transf. 52 (2009) 3805–3817.

[30] M. Şeşen, W. Khudhayer, T. Karabacak, A. Koşar, Compact nanostructure integrated pool boiler for microscale cooling applications, Micro Nano Lett. (2010).

[31] R. Chen, M.-C. Lu, V. Srinivasan, Z. Wang, H.H. Cho, A. Majumdar, Nanowires for enhanced boiling heat transfer., Nano Lett. 9 (2009) 548–53.

[32] a. K.M.M. Morshed, F. Yang, M. Yakut Ali, J. a. Khan, C. Li, Enhanced flow boiling in a microchannel with integration of nanowires, Appl. Therm. Eng. 32 (2012) 68–75.

[33] D. Saeidi, A.A. Alemrajabi, Experimental investigation of pool boiling heat transfer and critical heat flux of nanostructured surfaces, Int. J. Heat Mass Transf. 60 (2013) 440–449.

[34] A. Kaya, R. Demiryürek, E. Armağan, G. Ozaydin-Ince, M. Sezen, A. Koşar, Boiling heat transfer enhancement in mini/microtubes via polyhydroxyethylmethacrylate (pHEMA) coatings on inner microtube walls at high mass fluxes, J. Micromechanics Microengineering. 23 (2013) 115017.

[35] T. Çikim, E. Armagan, G. Ozaydin Ince, A. Kosar, Flow Boiling Enhancement in Microtubes With Crosslinked pHEMA Coatings and the Effect of Coating Thickness, J. Heat Transfer. 136 (2014) 081504.

[36] W. Frost, C.J. Kippenhan, Bubble growth and heat-transfer mechanisms in the forced convection boiling of water containing a surface active agent, Int. J. Heat Mass Transf. 10 (1967) 931–949.

[37] D.S. Wen, B.X. Wang, Effects of surface wettability on nucleate pool boiling heat transfer for surfactant solutions, Int. J. Heat Mass Transf. 45 (2002) 1739–1747.

[38] H. Jo, H.S. Ahn, S. Kang, M.H. Kim, A study of nucleate boiling heat transfer on hydrophilic, hydrophobic and heterogeneous wetting surfaces, Int. J. Heat Mass Transf. 54 (2011) 5643–5652.

[39] A.R. Betz, J. Jenkins, C.J. Kim, D. Attinger, Boiling heat transfer on superhydrophilic, superhydrophobic, and superbiphilic surfaces, Int. J. Heat Mass Transf. 57 (2013) 733–741.

[40] W.E. Tenhaeff, K.K. Gleason, Initiated and Oxidative Chemical Vapor Deposition of Polymeric Thin Films: iCVD and oCVD, Adv. Funct. Mater. 18 (2008) 979–992.

[41] G. Ozaydin-Ince, K.K. Gleason, Transition between kinetic and mass transfer regimes in the initiated chemical vapor deposition from ethylene glycol diacrylate, J. Vac. Sci. Technol. A Vacuum, Surfaces, Film. 27 (2009) 1135.

[42] M.E. Alf, A. Asatekin, M.C. Barr, S.H. Baxamusa, H. Chelawat, G. Ozaydin-Ince, et al., Chemical vapor deposition of conformal, functional, and responsive polymer films., Adv. Mater. 22 (2010) 1993–2027.

[43] K.K.S. Lau, K.K. Gleason, Initiated Chemical Vapor Deposition (iCVD) of Poly(alkyl acrylates): A Kinetic Model, Macromolecules. 39 (2006) 3695–3703.

[44] P. Larkin, Infrared and Raman Spectroscopy; Principles and Spectral Interpretation, Elsevier, 2011.

[45] K. Chan, K.K. Gleason, Initiated chemical vapor deposition of linear and cross-linked poly(2-hydroxyethyl methacrylate) for use as thin-film hydrogels., Langmuir. 21 (2005) 8930–9.

[46] M. Gupta, K.K. Gleason, Initiated chemical vapor deposition of poly(1H,1H,2H,2H-perfluorodecyl acrylate) thin films., Langmuir. 22 (2006) 10047–52.

[47] S. Kline, F. McClintock, Describing uncertainties in single-sample experiments, Mech. Eng. (1953).

[48] F. Incropera, D. Dewitt, Introduction to heat transfer, (1985).

[49] K.D. Cole, B. Çetin, The effect of axial conduction on heat transfer in a liquid microchannel flow, Int. J. Heat Mass Transf. 54 (2011) 2542–2549.

[50] G.L. Morini, Scaling Effects for Liquid Flows in Microchannels, Heat Transf. Eng. 27 (2006) 64–73.

[51] M. Kaviany, Principles of heat transfer in porous media, Springer Sci. Bus. Media. (2012).

[52] S. Daniel, M.K. Chaudhury, J.C. Chen, Fast drop movements resulting from the phase change on a gradient surface., Science. 291 (2001) 633–6.

[53] M.K. Chaudhury, G.M. Whitesides, How to make water run uphill., Science. 256 (1992) 1539–41.

[54] B. Bhushan, Biomimetics: lessons from nature--an overview., Philos. Trans. A. Math. Phys. Eng. Sci. 367 (2009) 1445–86.

[55] M. Nosonovsky, B. Bhushan, Multiscale friction mechanisms and hierarchical surfaces in nano- and bio-tribology, Mater. Sci. Eng. R Reports. 58 (2007) 162–193.

[56] Z.S. Saifaldeen, K.R. Khedir, M.F. Cansizoglu, T. Demirkan, T. Karabacak, Superamphiphobic aluminum alloy surfaces with micro and nanoscale hierarchical roughness produced by a simple and environmentally friendly technique, J. Mater. Sci. 49 (2013) 1839–1853.

[57] J. Ramilison, Surface factors influencing burnout on flat heaters, J. Heat Transfer. (1992) 287–290.

[58] T. Raad, J. Myers, Nucleation studies in pool boiling on thin plates using liquid crystals, AIChE J. (1971).

[59] P. Berenson, Experiments on pool-boiling heat transfer, Int. J. Heat Mass Transf. (1962).

[60] K. TORIKAI, K. SUZUKI, A. MIZUTA, Effect of surface roughness on boiling heat transfer, Therm. Non-Equilibrium Two-Phase Flow. 511 (1989).